Chalcogenide Letters Vol. 17, No. 2, February 2020, p. 69 - 76

SYSTEMATIZED AND SIMPLIFIED PROCESSING OF $CuInGaSe_2$ THIN FILMS TO BE APPLIED ON SOLAR CELLS

J. SASTRÉ-HERNÁNDEZ[a,*], R. MENDOZA-PÉREZ[b],
M. L. ALBOR-AGUILERA[a], D. JIMÉNEZ-OLARTE[c], G. SANTANA[e],
M. TUFIÑO-VELÁZQUEZ[a], A. MORALES-ACEVEDO[d],
G. CONTRERAS-PUENTE[a]
[a]*ESFM-IPN, Physics Department, U.P.A.L.M., San Pedro Zacatenco, CDMX, 07738, Mexico*
[b]*UACM, Av. Prolongación San Isidro 151, Col. San Lorenzo Tezonco, CDMX, 09790, Mexico*
[c]*ESIME-IPN, Section of Postgraduate Studies and Research, U.P.A.L.M., San Pedro Zacatenco, CDMX, 07738, Mexico*
[d]*CINVESTAV-IPN, Electrical Engineering Department, Av. IPN No. 2508, CDMX, 07360, Mexico*
[e]*Institute of Materials Research, UNAM, Coyoacán, Mexico*

Results of processing and characterization of $Cu(In,Ga)Se_2$ (CIGS) thin films growth by thermal co-evaporation with adequate physical properties to be used in solar cells are presented in this work. Cadmium Sulfide (CdS) as window material with 40 nm of thickness were deposited by chemical bath deposition (CBD) technique. A Molybdenum (Mo) layer was deposited as back contact on CIGS solar cells. Different CIGS thin films were processed by a simplified co-evaporation technique and revealed a good polycrystalline quality with an alfa-chalcopyrite phase. The stoichiometry of the CIGS thin films can be accurately controlled using a fully automated single vacuum photovoltaics manufacturing system. Automated system operations (ASO) is the set of software and hardware that allows computer systems, network devices or machines to function without any manual intervention. ASOs allow computer systems to work without a human operator physically located at the site where the system is installed. CIGS solar cells fabricated in this work, showed photovoltaic efficiencies close to 11 %.

(Received October 28, 2019; Accepted February 14, 2020)

Keywords: Simplified process, CIGS thin films, Photovoltaic devices

1. Introduction

Recently, CuIn1-xGaxSe2 (CIGS) and CuInSe2 (CIS) semiconductor materials have been thoroughly investigated as suitable absorber layers for second generation solar cells, due to their large radiation tolerance, excellent chemical stability and large optical absorption coefficients [1-3]. The addition of Ga into CIS material does not modify the direct band gap nature. CIGS has a high absorption coefficient of ~ 1×105 cm-1 for energies larger than 1.4 eV, promising its application as absorber layer on photovoltaics (PV) thin films technology. A 90 % of solar spectrum can be absorbed using ~ 1.5 µm to 2 µm of CIGS layer thickness, yielding lighter solar cells and saving material [4]. Thus, CIGS-based solar cells are promising for long durability, low fabrication cost and large conversion efficiency [5, 6].

The first CIGS-based solar cell was reported by Kazmerski *et al.* in 1976, with an efficiency of 4.5 %[7]. Nowadays, laboratory record efficiency of 22.9 % has been reported by Jackson *et. Al*, while industry record efficiency of 23.35 % has been recently reported by Solar Frontier[3, 8]. Thus, CIGS is a promising material in order to achieve even higher efficiencies and better PV-performance. It can be carried out with new technical and engineering improvements,

* Corresponding author: jsastrehdz@gmail.com

like for example CIGS-post deposition treatments with alkaline elements, inclusion of Mo selenides ultra-thin layers to get a better band alignments, sulphur-selenide compounds and tandem cells with perovskite technology [3, 9, 10]. On the other hand, CdS is an II-VI compound, n-type semiconductor with band gap energy of 2.45 eV. It is used to fabricate CIGS heterojunction. Carrier density of CdS is higher than in CIGS, the depletion field is completely in CIGS layer where it generates electron-hole pairs; so that polycrystalline, optical and electrical properties of CIGS thin films are very important. These properties depend of two factors: deposition method and thermal annealing.

One of the aims of this research is to study the physical properties of CIGS thin films can be controlled using an automated vacuum photovoltaics manufacturing system and its influence in the photovoltaic efficiency of the processed solar cells. The patented idea of three stage mode CIGS growth technique by Hasoon *et. al*.,[11, 12] where the precursors are not evaporated at the same time and using different temperatures ramps for each material was not considered in this work. The automated and uniform processing of the absorber layer using our unique-homemade vacuum manufacturing tool which allowed us a good control of the rates of growths during the processing of the CIGS thin film, is also described. Results about the growth conditions of CIGS layers and their structural, optical and electrical properties are presented in this work. CIGS/CdS solar cells were fabricated and electrically characterized.

2. CIGS layer growth and characterization

2.1. Implementation of CIGS growth automated process

A simplified and accessible process was implemented and tested to remark the difference between highly efficient technology and low-cost manufacturing. Manufacturing tool is a fully automated tool handled by a program developed in LabVIEW 2017. CIGS photovoltaic technology known as Knudsen cells using Molecular Beam Epitaxy (MBE) technology was modified by integrating a temperature control (± 0.1 °C) in the growth process what makes the difference regarding the conventional system [7]. A schematic diagram of controlled components of system is shown in Figure 1. An advantage of this system is that all deposition parameters can be established and modified while the program is running. Temperature and pressure parameters inside of evaporation chamber are monitored frequently and experimental graph as time function is registered during the growth process. All experimental data are recorded automatically for further analysis. Chamber pressure is controlled by two automated vacuum pumps system; calibrated pirani and cathode-cold were used. Low-cost automated system is capable to modifiy the temperature parameter as a function of time for each Knudsen cell and substrate temperature at the same time. Shutters aperture and growth temperature can be programed individually allowing a sequential and controlled growth of Cu, In, Ga and Se in co-evaporation process. In order to guarantee uniform thickness along the sample, the substrate is enabled to rotate at an angular speed (~10 RPM) defined by the user.

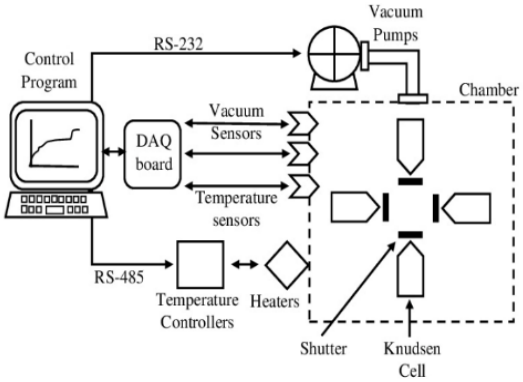

Fig. 1. Automated setup of CIGS system.

2.2 CIGS thin films growth

High purity Cu (Kurt Lesker, 99.999 %), Ga (Alfa Aesar, 99.9999 %), Se (Kurt Lesker, 99.999%) and In (Kurt Lesker, 99.999%) starting materials were put into Knudsen cells in order to deposit CIGS thin films by one-stage thermal co-evaporation on soda lime glass substrates with a Mo sputtered layer (~0.7 μm of thickness). All CIGS samples were processed at 10^{-6} Torr with substrate temperature of 500 ^{o}C during 30 min; this control was programmed in the same run processed. During the one-stage process deposition of each of the CIGS thin film the source growth temperatures (growth rates) for each material are described in the Table 1.

Table 1. Experimental parameters of CIGS growth.

Samples	$T_{Cu}(°C)$	$T_{Ga}(°C)$	$T_{In}(°C)$	$T_{Se}(°C)$
A	1300	1100	930	215
B	1300	1120	930	215
C	1300	1110	930	215
D	1300	1100	940	215
E	1290	1100	940	215
F	1310	1120	930	210

For CIGS samples X-Ray diffraction (XRD) measurements were taken using a Siemens Mod. D-5000 diffractometer using the Cu Kα ($\lambda = 1.54$ Å) radiation at 40 kV and 20 mA, in a 2θ range of 20 – 60°. Morphological and chemical quantification of CIGS samples were analyzed by using scanning electron microscopy (SEM) and energy dispersive spectroscopy (EDS) techniques, respectively. A JEOL 6360 LV scanning electron microscope equipped with an Oxford Instrument Energy 200 EDS analytical system, was used to obtain the micrographs with an applied voltage of 20 kV. Photoluminescence (PL) studies were done from 6.5 to 120 K, using a He-Ne laser (632.8nm) as an excitation source with an InGaAs photodiode used as a detector. Raman studies were performed using a Horiba Jobin Yvon (HR) LabRaman Spectrometer equipped with a microscope and a 17 mW He-Ne Laser. This system has a spectral resolution value of 1 cm^{-1} and a spatial resolution of 12 μm (100X objective).

CdS semiconductor thin films were deposited on CIGS substrates by Chemical Bath Deposition (CBD) technique, using a precursor solution $CdCl_2$ (0.1 M), NH_4Cl (0.2 M), NH_3 (2 M) and $(NH_2)_2CS$ (0.3 M). CdS thin layers of 40 nm were obtained. CIGS/CdS junction samples was thermally annealed in air at 450 $^{\circ}$C for 60 min.

3. Results and Discussions

XRD measurements show sharp and well-defined peaks, as it is observed in Fig. 2, indicating good crystalline quality. The (112) peak is slightly shifted towards smaller angle in agreement with the stoichiometry of CuIn0.7Ga0.3Se2 [13]. Using the Scherrer equation, a crystal size of 40 nm was calculated.

No preferential orientation is observed, as a consequence of the sample poly crystallinity. Several reflections revealing the chalcopyrite structure are observed, namely (112), (220)/(204), (211), (312) and (103) according to JCPDS-35-1102 Tetragonal CuIn0.7Ga0.3Se2. The peak located at 40.3 degrees corresponds to the (110) Mo layer. The lattice parameters *a* and *c* have been calculated, yielding *a = 5.73 Å* and *c = 11.38 Å*. This in turn yields a tetragonal distortion $\Delta = 2 - \frac{c}{a} = 0.0139 > 0$, indicating compressive strain.

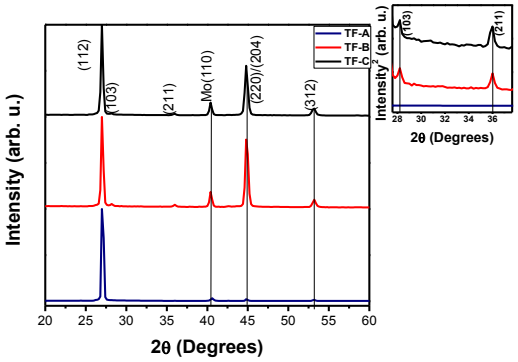

Fig. 2. Representative XRD diffractograms for CIGS samples.

In Fig. 3 representative surface SEM images are shown for samples C, D and E, respectively, together with a representative cross section image of F sample.

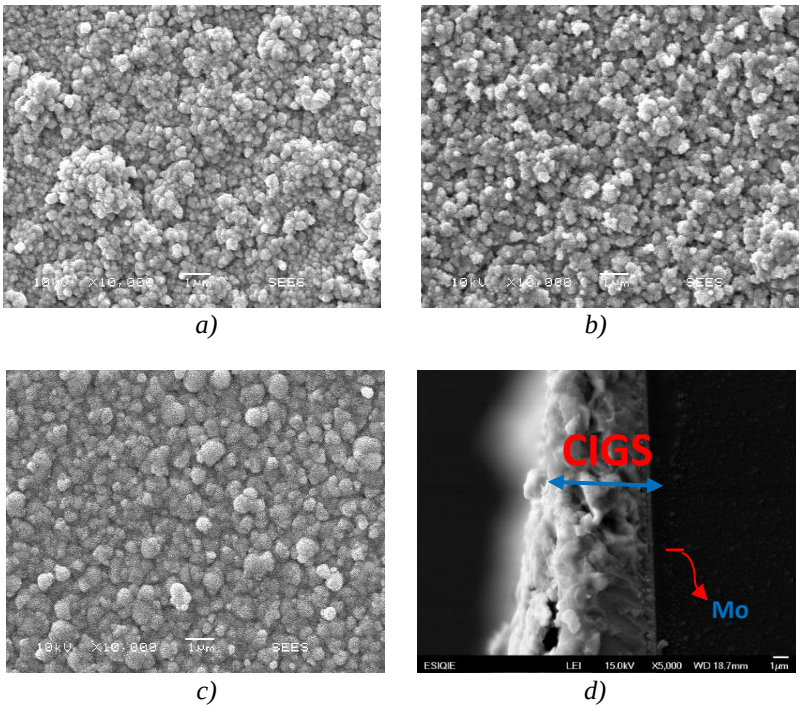

Fig. 3. Representative SEM images for :
a) sample C, b) sample D c) sample E,
d) cross section image for sample F.

Fig. 3 a) to d) SEM images exhibit small grain (~ 1µm) with a good uniform coverage. Apparently, the CIGS films did not experience liquid-phase-assisted re-crystalline process although the growth temperature was beyond 523 °C. Cross-section SEM Fig. 3 F) reveals a film thickness around of ~ 3.5 µm. Samples with a reduction on the amount of Cu presented a larger grain size and higher compactness. By using the experimental parameters of growths shown in Table 1, several X = *[Ga]/([In] +[Ga]) = 0.28, 0.34, 0.35* and Y = *[Cu]/([In] + [Ga])= 0.85, 0.83, 0.94* concentrations were obtained by varying the temperatures of the gallium and indium source. EDS results are summarized in Table 2.

Table 2. EDS results.

Sample	Chemical composition (at %) by EDS				Composition ratio	
	Cu[at %]	In[at %]	Ga[at %]	Se[at %]	Ga/(In+Ga)	Cu/(In+Ga)
A	22.1	18.8	7.3	51.8	0.28	0.85
B	21.3	16.7	8.9	53.7	0.35	0.83
C	23.0	16.2	8.2	53.5	0.34	0.94
D	22.9	19.4	6.5	51.1	0.25	0.88
E	21.5	19.4	6.5	52.3	0.25	0.83
F	24.5	16.9	9.7	48.9	0.37	0.92

Fig. 4 shows a representative PL spectrum of the C sample as function of the temperature; the spectra reveals four distinctive signals, namely at 1.04 eV, 1.12 eV, 1.18 eV and 1.25 eV for temperatures below 77 K. Using a band gap bowing model as a function of the Ga concentration reported by Alonso M *et al.* [14], a band gap edge of 1.25 eV was calculated for this sample, in reasonable agreement with the largest PL signal observed in Fig. 4. Thus, we attribute it to exciton recombination in the near band edge. It can be observed in Fig. 4 that the FWHM of the emission peaks at 1.12 and 1.18 eV decreased as the emission intensity decreased, suggesting thermalization effects. At the same time, the energy difference with the band edge emission (1.25 eV), is 130 meV and 70 meV, for signals at 1.12 eV and 1.18 eV, respectively, suggesting us that both emissions are related to non-shallow defects levels. Zott *et al.*[15] reported donor activation energy of 160 meV for *InCu* and donor activation energy of 80 meV for *VSe*, while an acceptor activation energy of 40 meV for *VCu* was reported by Massé *et al.*[16] Hence, we assigned the 1.12 eV and 1.18 eV to donor-acceptor pair (DAP) transitions.[17] Finally, the signal at 1.03 eV has an energy difference of 220 meV with the band gap edge. This energy is between the donor-acceptor transition of level of VSe –VCu, theoretically predicted by Lany and Zunger, hence we tentatively assigned to it.[18]

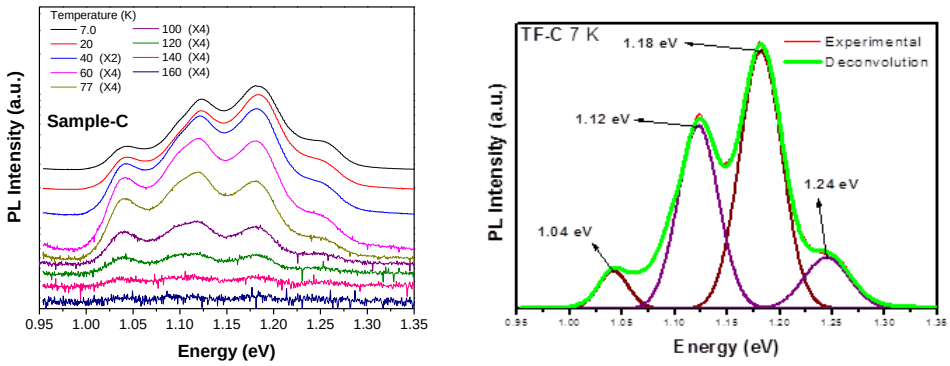

Fig. 4. Representative PL image and deconvolution results at 7 K for sample C.

The representative Raman spectra are shown in Fig. 5.Three distinctively Raman signals can be observed in Fig. 5, namely at 174, 220 and 250 cm-1. The signal at 174 cm-1 is due to the A1 mode due to the vibration of Se with Cu, In and Ga atoms at rest, while the Raman signals as 220 cm-1 and 250 cm-1 correspond to the B2 and E1 modes, due to the combined motion of all atoms.[19] These values are shifted from the Raman CIS modes due to low Ga incorporation. It is noticed that the FWHM of the A1 mode decreases with decreasing Ga content, in reasonable agreement with better crystallinity, when the disorder in the CIGS film is reduced.

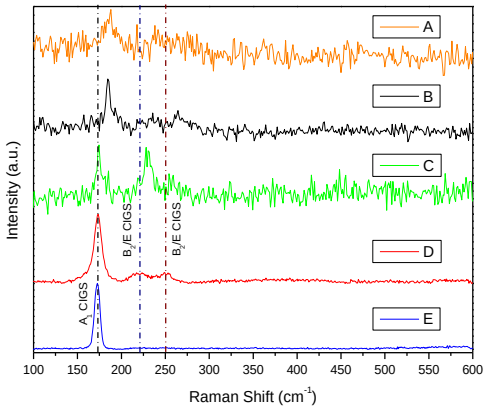

Fig. 5. Representative Raman spectra for the CIGS thin films processed.

4. Solar cell processing and performance

Four photovoltaic devices, D-1, D-2, D-3 and D-4 were processed using a classical substrate configuration Mo/CIGS/CdS/i-ZnO/ZnO:Al/Ni-Al. These devices were fabricated using similar experimental parameters as F layer reported above (Table 1 and 2) for the absorber material, because F CIGS thin film showed the best [Ga]/([In]+[Ga]) and [Cu]/([In]+[Ga]) critical parameters for solar cells according to the literature.[3]

CdS thin films were deposited on CIGS sample and thermally annealing in air, to conclude the photovoltaics structures. Afterwards ZnO and ITO were deposited via rf-sputtering and the metal contact was Ni/Al deposited by thermal evaporation, using a defined patterned grid. Fig. 6 shows the J-V and normalized External Quantum Efficiency (EQE) curves for the devices. The electrical output parameters of the solar cells are summarized in Table 3.

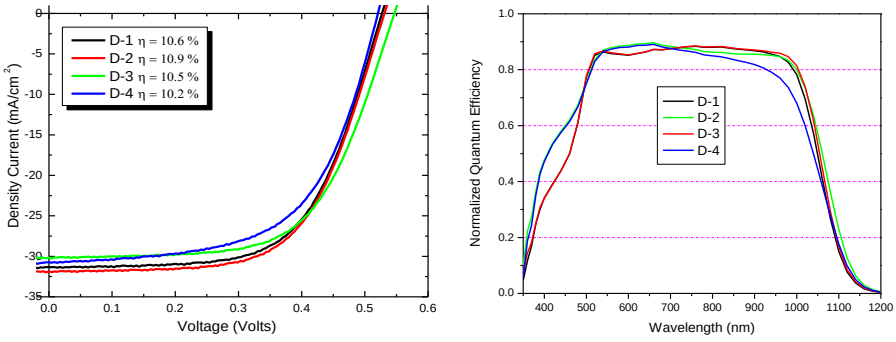

a) *b)*

Fig. 6 a) J-V curves and b) EQE for the fabricated devices.

Table 3. J-V parameters summary data for fabricated CIGS devices.

Device	Electrical solar cell parameters						
	Area (cm^2)	Rs (Ωcm^2)	Rsh (Ωcm^2)	Voc (mV)	Jsc (mA/cm^2)	FF (%)	η (%)
D-1	0.47	3.9	955	532	31.1	64	10.6
D-2	0.47	3.8	759	536	31.7	64	10.9
D-3	0.47	3.8	454	558	29.9	63	10.5
D-4	0.47	2.9	256	540	30.6	62	10.2

The last results reveal the quality and repeatability of the all solar cells devices processed in this work, with a slight affection in the series resistance due to the used grid and the subsequent contact treatments are not optimized yet. D-1 and D-2 cells showed the best solar conversion efficiencies due to an improvement in the photo-generated electrical current in the CdS film region according to the EQE measurements, although the device D-4 do not collect efficiently in the long wavelengths.

5. Conclusions

We have made a study of CIGS solar cells, showing that the best PV-performance was obtained by the one was CIGS processed by the co-evaporation technique, with the growth conditions of sample F, using a unique absorber layer manufacturing tool. [20]

Four CIGS based solar cells were compared in this work. In the best one photovoltaic device (D-2) the CdS and CIGS layers has optical and electrical properties that shows that both have good properties. According to the EQE curves a better electron-hole pairs generated collection is observed at wavelengths bellow ~500 nm for D-2 case. In our study, we have shown that we can achieve efficient solar cells, using an innovative manufacturing tool and a well-known standard process. It is important to mention that the thickness ratio of the TCO and the buffer layer should be optimized, as well as the structure of the contacts in order to improve the short-circuit current and the fill factor of the devices. The hardware and process has been optimized to make over 10% efficient CIGS/CdS cells with the half of the growth rates reported by Takuya Kato et al. and with good reproducibility, according to the almost the same efficiencies values reported in this work. [9]

Acknowledgements

The National Council for Science and Technology (CONACyT) supported this work, grants 47587. J. Sastré-Hernández acknowledgments to IPN for the support under SIP-20196099 and SIP-20200830 projects. M. Tufiño-Velázquez acknowledgments to IPN for the support under SIP-20195128 and SIP-20200510 projects. Special thanks for technical support to Ing. Benito Ortega Nájera.

References

[1] M. Kernell, M. Ritala, M. Leskelä, Crit. Rev. Solid State Mater. Sci **30**, 1 (2005).
[2] S. Niki, M. Contreras, I. Repins, M. Powalla, K. Kushiya, S. Ishizuka, K. Matsubara, Prog. Photovolt. Res. Appl. **18**, 453 (2010).
[3] Solar Frontier (2019, January 17), Solar Frontier Achieves World Record Thin-Film Solar Cell Efficiency of 23.35%. Retrieved from http://www.solar-frontier.com/eng/news/2019/0117_press.html.
[4] S. Yasar, S. Kahraman, S. Cetinkaya, S. Apaydin, I. Bilican, I. Uluer, Optik **127**, 8827 (2016).
[5] S. Hegedus, Prog. Photovolt. Res. Appl. **14**, 393 (2006).
[6] Takuya Kato, Jyh-Lih Wu, Yoshiaki Hirai, Hiroki Sugimoto, Veronica Bermudez, IEEE Journal of Photovoltaics **9**(1), 325 (2019).
[7] L. L. Kazmerski, F. R. White, G. K. Morgan, Appl. Phys. Lett. **29**, 268 (1976).
[8] Philip Jackson, Roland Wuerz, Dimitrios Hariskos, Erwin Lotter, Wolfram Witte, Michael Powalla**,** Phys. Status Solidi RRL **10**(8), 583 (2016).
[9] Takuya Kato, Atsushi Handa, Takeshi Yagioka, Tetsuya Matsuura, Kentarou Yamamoto, Shougo Higashi, Jyh-Lih Wu, Kong Fai Tai, Homare Hiroi, Takashi Yoshiyama, Tetsuya Sakai, and Hiroki Sugimoto, IEEE Journal of Photovoltaics **7**(6), 1773 (2017).

[10] Tomas Feurer, Patrick Reinhard, Enrico Avancini, Benjamin Bissig, Johannes Löckinger, Peter Fuchs, Romain Carron, Thomas Paul Weiss, Julian Perrenoud, Stephan Stutterheim, Stephan Buecheler, Ayodhya N. Tiwari, Prog. Photovolt: Res. Appl. **25**, 645 (2017).
[11] F. S. Hasoon, Y. Yan, H. Althani, K. M. Jones, H. R. Moutinho, J. Alleman, M. M. Al-Jassim, R. Noufi, Thin Solid Films **387**, 1 (2001).
[12] Nowshad Amin, J. Applied Sci. **11**(3), 401 (2011).
[13] C. J. Hibberd, M. Ganchev, M. Kaelin, S. E. Dann, G. Bilger, H. U. Upadhyaya, A. N. Tiwari, Thin Solid Films **51**, 2235 (2009).
[14] M. Alonso, M. Garriga, C. A. Durante Rincón, E. Hernández, M. León, Appl. Phys. A **74**, 659 (2002).
[15] S. Zott, K. Leo, M. Ruck, H.-W. Schock, Appl. Phys. Lett. **68**, 1144 (1996).
[16] G. Massé, E. Redjai, J. Appl. Phys. **56**, 1154 (1984).
[17] N. Rega S. Siebentritt, J. Albert, S. Nishiwaki, A. Zajogin, M. Ch. Lux-Steiner, R. Kniese, M. J. Romero, Thin Solid Films **480-481**, 286 (2005).
[18] S. Lany, A. Zunger, J. Appl. Phys. **100**, 113725 (2006).
[19] W. Witte, R. Kniese, M. Powalla, Thin Solid Films **57**, 867 (2008).
[20] M. L. Albor Aguilera, J. M. Flores Márquez, M. A. González Trujillo, C. Hernández Vásquez, G. Contreras Puentea, C. Mejía García, G. Rueda Morales, Rev. Mex. Fis. **62**, 129 (2016).
[21] A. E. Abken, D. P. Halliday, K. Durose, J. Appl. Phys. **105**, 064515 (2009).